

Article

Synthesis and Crystallographic Characterization of Heteroleptic Ir(III) Complexes Containing the *N*-oxide Functional Group and Crystallographic Characterization of Ir(III) *N*-oxide Precursors

Emily E. Stumbo¹, Emerald K. Hodge¹, Matthew Williams², Diana A. Thornton², Colin D. McMillen^{3,*} 
and Jared A. Pienkos^{1,*}

¹ Department of Chemistry and Physics, The University of Tennessee at Chattanooga, Chattanooga, TN 37403, USA

² Department of Chemistry, Virginia Tech, Blacksburg, VA 24060, USA

³ Department of Chemistry, Clemson University, Clemson, SC 29634, USA

* Correspondence: cmcmill@clemson.edu (C.D.M.); jared-pienkos@utc.edu (J.A.P.)

Abstract: The *N*-oxide functional group has been exploited for synthetic strategies and drug design, and it has been utilized in imaging agents. Herein, we present rare examples of neutral heteroleptic cyclometallated Ir(III) compounds that contain an uncoordinated *N*-oxide functional group. These species, along with others described within, were verified by NMR, EA, HRMS, and single-crystal X-ray analysis. *N*-oxide-containing Ir(III) species were prepared selectively in high yields > 66% from chloro-bridged Ir(III) dimers with Acipimox, a picolinate-type ligand containing the *N*-oxide functional group. Non-*N*-oxide analogs were synthesized in a similar fashion (yields > 77%). Electrochemical comparison (cyclic voltammetry) indicates that the presence of an *N*-oxide functional group anodically shifts the reduction potential, suggesting that the *N*-oxide is acting as an electron-withdrawing group in these species. Crystallographic studies were pursued to examine the coordination behavior of these *N*-oxides compared to their non-oxidized congeners. The Ir(III) complexes with Acipimox indeed leave the *N*-oxide uncoordinated and exposed on the complexes. The uncoordinated *N*-oxide group is influential in directing the packing structures of these complexes directly through C-H...O and O... π interactions at the *N*-oxide. The crystallographic characterization of cationic Ir(III) compounds with uncoordinated nitrogen atoms is also presented. The C-H...N interactions between these complexes form a variety of dimers, finite chains, and continuous chains. Future work will focus on functionalizing the cationic Ir(III) species into their corresponding *N*-oxide derivatives and rigorously characterizing how the *N*-oxide functional group impacts the optical properties of transition metal compounds in both cationic and neutral complexes.

Keywords: cyclometallated iridium species; *N*-oxide transition metal complex; heteroleptic iridium complexes; coordination chemistry; crystal structure



Citation: Stumbo, E.E.; Hodge, E.K.; Williams, M.; Thornton, D.A.; McMillen, C.D.; Pienkos, J.A. Synthesis and Crystallographic Characterization of Heteroleptic Ir(III) Complexes Containing the *N*-oxide Functional Group and Crystallographic Characterization of Ir(III) *N*-oxide Precursors. *Crystals* **2024**, *14*, 281. <https://doi.org/10.3390/cryst14030281>

Academic Editor: Vladimir P. Fedin

Received: 29 February 2024

Revised: 8 March 2024

Accepted: 11 March 2024

Published: 16 March 2024



Copyright: © 2024 by the authors. Licensee MDPI, Basel, Switzerland. This article is an open access article distributed under the terms and conditions of the Creative Commons Attribution (CC BY) license (<https://creativecommons.org/licenses/by/4.0/>).

1. Introduction

N-oxide-containing compounds have been exploited for various applications, including synthetic intermediates [1], drug molecules [2], and imaging agents [3–5]. The *N*-oxide functional group can be cleaved in a hypoxic environment. This has been utilized in the design of various prodrugs and imaging agents that change form in tumor cells, where the concentration of oxygen is low [2,4–7]. For instance, an *N*-oxide on the chemotherapeutic Tirapazamine (Figure 1) is cleaved under hypoxic conditions to generate reactive radical species [6]. Regarding imaging agents, Knox et al. have shown that BODIPY dyes containing cleavable *N*-oxides can be exploited for ratiometric imaging [4,5].

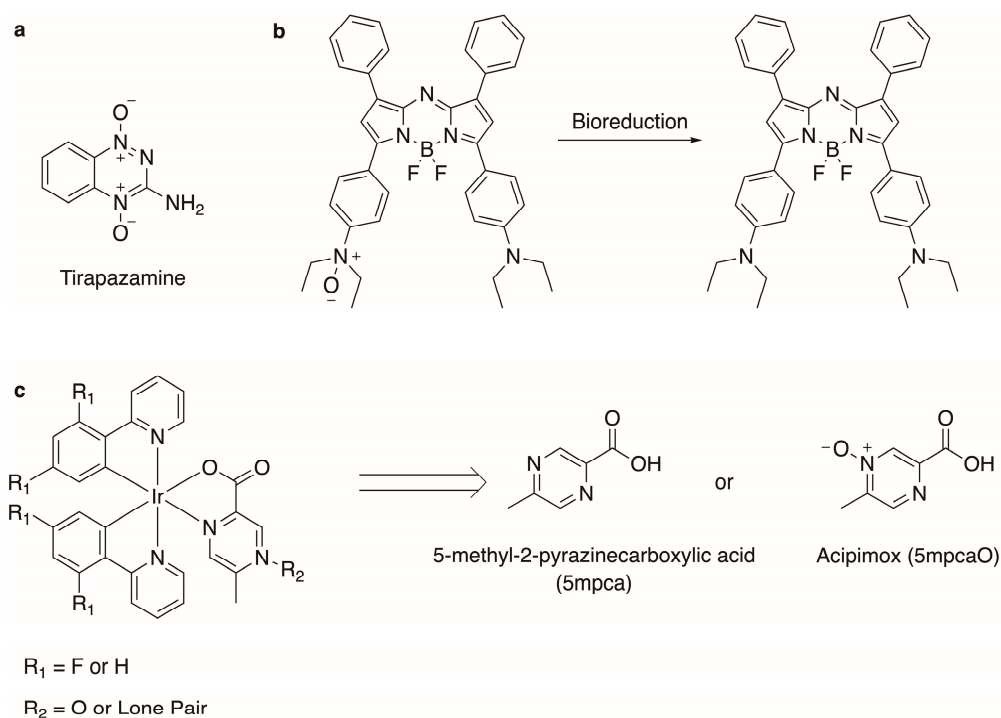


Figure 1. Biologically relevant N-oxide-containing compounds: (a) Tirapazamine is utilized as a chemotherapeutic [6]; (b) BODIPY dyes are utilized in ratiometric imaging [4,5]; (c) synthetic scheme for neutral Ir(III) compounds and abbreviations used within.

Recently, transition metal compounds have gained the attention of the scientific community as imaging agents due to their typically large Stokes shift, long fluorescent lifetimes, and tunable luminescence [8–10]. To develop other imaging agents, mainly to monitor hypoxia, we envisioned a strategy that parallels the work of Knox et al. [4,5] using transition metal compounds that contain *N*-oxide functional groups instead of BODIPY dyes. Of interest are cyclometallated Ir(III) systems because of their ability to detect hypoxia in animals [11]. However, cyclometallated Ir(III) complexes containing external *N*-oxide groups on heterocyclic ligands have not been extensively structurally characterized, with one reported example describing a TEMPO radical [12]. More commonly, Ir(III) complexes involving a heterocyclic *N*-oxide ligand coordinate via the oxygen atom of the *N*-oxide group [13–19]. The tendency to coordinate the oxygen atom of a heterocyclic *N*-oxide group is generally favored in most transition metal complexes [20–23], largely due to the hardness of the *N*-oxide as a donor. Strategies for orienting the oxygen atom of the *N*-oxide group externally on a metal complex (that is, not coordinated to the metal) may include utilizing ligands with favorable coordination sites away from the *N*-oxide or oxidizing the exposed external nitrogen atom of a coordinated ligand [24–32]. For the former, ligands such as 5-methylpyrazine-2-carboxylate (5 mpca) and its corresponding *N*-oxide (Acipimox, 5 mpcaO, Figure 1) may be promising [33]. For the latter, crystallographically characterizing those complexes where nitrogen atoms are external to the complex and available for oxidation is an appropriate first step.

Herein, we report rare examples of structurally characterized cyclometallated Ir(III) species that have an *N*-oxide functional group that is not involved in coordination to the metal center. Ultimately, our group desires to exploit these compounds as imaging agents. In this initial report, we focus on the structural characterization of these derivatives and other Ir(III) compounds that can serve as precursors for other unbound *N*-oxide-containing transition metal species. Although a number of these other Ir(III) complexes having non-oxidized external nitrogen atoms have been reported in the synthetic literature, they have heretofore not been studied crystallographically. Electrochemical data are also presented

to demonstrate that the presence of an *N*-oxide functional group can be used to tune the electronic properties of a transition metal center.

2. Materials and Methods

2.1. General Methods

UV-Vis: The reported molar extinction coefficients were obtained through the same method for complexes 1–4. An Agilent Cary 60 UV-Vis spectrometer equipped with a xenon lamp was utilized for data collection. Sample solutions were prepared by weighing ~5 mg of each complex and creating a stock solution using MeOH (100 mL). Aliquots from this stock solution were used to prepare 90–10% concentrations, yielding a total of 10 solutions. A background was obtained using MeOH in a 1 cm quartz cuvette. Sample collection was performed at a 24,000 nm/min scan rate within a 300 to 700 nm window. The absorption maxima at each peak were plotted against a concentration curve to obtain molar extinction coefficients.

Cyclic voltammograms: Data were recorded using a BASi epsilon electrochemical workstation and a BASi cell stand. Conditions for data collection: [Ir]~1 mM in CH₂Cl₂ (0.1 M TBAPF₆, where TBA = tetrabutylammonium), glassy carbon working electrode, and Ag/Ag⁺ reference electrode. The *x*-axis reports voltages vs. ferrocene (FcH) as determined by running a voltammogram of FcH before and after data collection.

NMR spectra: ¹H NMR, ¹⁹F NMR, and ³¹P NMR spectra were recorded on a JEOL ECX 400 MHz spectrometer. ¹H NMR resonances were referenced against tetramethylsilane using residual proton signals. Standards were run for ¹⁹F NMR (fluorobenzene) and ³¹P NMR (triphenylphosphine) prior to data acquisition: fluorobenzene (−113 ppm, CDCl₃, and d-DMSO) and triphenylphosphine (−6 ppm, d-DMSO). All NMR spectra were acquired at room temperature (solutions of the complex in CDCl₃ for 1–4, and in DMSO-*d*₆ for 6).

HRMS: Mass spectra were obtained with an Agilent accurate-mass 6520B Q-TOF mass spectrometer operating in positive-ion mode with a 3500 V capillary voltage and 120 V fragmentor voltage. The dual-spray electrospray ionization (ESI) source operated with a nebulizer pressure of 40 psi and 340 °C N₂ drying gas flowing at 12 L/min. The instrument was calibrated with the Agilent ESI-L tuning mix. During measurements, a reference solution containing ammonium trifluoroacetate, purine ([M + H]⁺ 121.0509) and hexakis (1H, 1H, 3H-tetrafluoropropoxy)phosphazine (HP-0921, C₁₈H₁₈F₂₄N₃O₆P₃) ([M + H]⁺ 922.0098) was continuously introduced into the ESI source to allow for internal mass calibration. Samples were introduced into the mass spectrometer, without chromatographic separation, in a mobile phase consisting of 0.1% formic acid in methanol at a flow rate of 0.300 mL/min. Mass spectra were analyzed using MassHunter Qualitative Analysis Software (B.06 and B.08, Agilent, Santa Clara, CA, USA).

2.2. Synthesis

All solvents and reagents were used as received. [(ppy)₂Ir(μ-Cl)]₂ (where Hppy = 2-phenylpyridine) and [(dfppy)₂Ir(μ-Cl)]₂ (where Hdfppy = 2-(2'-4'-difluorophenyl)pyridine) were prepared according to previously reported methods [34].

General procedure 1 (GP1) for the preparation of Ir(C[^]N)₂(N[^]O) derivatives (where C[^]N = ppy or dfppy and N[^]O = a picolinic acid derivate) was as follows: For [(C[^]N)₂Ir(μ-Cl)]₂, 3 equivalents of the appropriate N[^]O ligand, and 6 equivalents of K₂CO₃ were added in an oven-dried pressure tube with acetone (~20 mL). After sparging the mixture with N₂, the pressure tube was sealed, and the reaction mixture was heated to 60 °C overnight, (~15 h). After cooling, the solvent was removed from the mixture, and the product was purified using a SiO₂ column and eluted with 5% MeOH/95% CH₂Cl₂. (Note: the column was typically packed with CH₂Cl₂ and CH₂Cl₂ could be initially used as an eluant to remove the excess ligand.) Fractions containing the product (as indicated by luminescent spots on the TLC) were dried in vacuo, resulting in a yellowish powder. The resulting solid was sonicated with hexanes (~10 mL), collected using vacuum filtration, and washed with hexanes.

Compound 1, GP1: [(dfppy)₂Ir(μ-Cl)]₂ (0.2004 g, 0.165 mmol), 5-methylpyrazine-2-carboxylic acid 4-oxide, Acipimox (0.0761 g, 0.494 mmol), K₂CO₃ (0.1363 g, 0.986 mmol), and acetone (23 mL) yielded 0.1588 g, 0.219 mmol, 66%. ¹H NMR (400 MHz, CDCl₃) δ 8.81 (s, 1H), 8.66 (ddd, J = 5.8, 1.7, 0.8 Hz, 1H), 8.27 (dddd, J = 10.4, 9.2, 2.2, 1.1 Hz, 2H), 7.85–7.76 (m, 2H), 7.64 (ddd, J = 5.8, 1.7, 0.8 Hz, 1H), 7.53–7.49 (m, 1H), 7.24 (ddd, J = 7.3, 5.8, 1.4 Hz, 1H), 7.06 (ddd, J = 7.4, 5.8, 1.4 Hz, 1H), 6.47 (ddd, J = 12.3, 9.1, 2.4 Hz, 1H), 6.40 (ddd, J = 12.5, 9.1, 2.4 Hz, 1H), 5.78 (dd, J = 8.5, 2.4 Hz, 1H), 5.49 (dd, J = 8.7, 2.4 Hz, 1H), 2.34 (s, 3H). ¹⁹F NMR (376 MHz, CDCl₃) δ −106 (dd, J = 9.35, 19.38 Hz, 1F), −107 (dd, J = 9.30, 19.47 Hz, 1F), −109 (t, J = 11.57 Hz, 1F), −110 (t, J = 11.91 Hz, 1F). UV-Vis λ_{max} (ε M^{−1}cm^{−1}): 318 nm (16071), 375 (6451.8). HRMS (found, calculated): [C₂₈H₁₇F₄IrN₄O₃ + H]⁺ (727.0951, 727.0940), [C₂₈H₁₇F₄IrN₄O₃ + Na]⁺ (749.0763, 749.0759). Elemental analysis (found, calculated) for C₂₈H₁₇F₄IrN₄O₃·1/2 H₂O, C (45.99, 45.78), H (2.60, 2.47), N (7.23, 7.63). Crystals were grown using vapor–vapor diffusion using THF/acetone as the dissolving solvent and pentane as the precipitating solvent.

Compound 2, GP1: [(dfppy)₂Ir(μ-Cl)]₂ (0.2025 g, 0.167 mmol), 5-methyl-2-pyrazinecarboxylic acid (0.0694 g, 0.502 mmol), K₂CO₃ (0.1372 g, 0.992 mmol), and acetone (30 mL) yielded 0.1824 g, 0.257 mmol, 77%. ¹H NMR (400 MHz, CDCl₃) δ 9.37 (d, J = 1.3 Hz, 1H), 8.70 (ddd, J = 5.7, 1.6, 0.8 Hz, 1H), 8.31 (dt, J = 8.1, 1.9 Hz, 1H), 8.29–8.24 (m, 1H), 7.82 (ddt, J = 6.7, 5.8, 2.1 Hz, 2H), 7.55 (dd, J = 1.3, 0.6 Hz, 1H), 7.41 (ddd, J = 5.8, 1.6, 0.8 Hz, 1H), 7.23 (ddd, J = 7.3, 5.8, 1.4 Hz, 1H), 7.02 (ddd, J = 7.3, 5.8, 1.4 Hz, 1H), 6.51 (ddd, J = 12.4, 9.2, 2.4 Hz, 1H), 6.42 (ddd, J = 12.5, 9.2, 2.4 Hz, 1H), 5.81 (dd, J = 8.5, 2.4 Hz, 1H), 5.49 (dd, J = 8.7, 2.4 Hz, 1H), 2.58 (s, 3H). ¹⁹F NMR (376 MHz, CDCl₃) δ −106 (dd, J = 10.00, 18.88 Hz, 1F), −107 (dd, J = 10.07, 19.28 Hz, 1F), −109 (t, J = 11.70 Hz, 1F), −110 (t, J = 11.70 Hz, 1F). UV-Vis λ_{max} (ε M^{−1}cm^{−1}): 313 nm (13741), 371 nm (5154.4). HRMS (found, calculated): [C₂₈H₁₇F₄IrN₄O₂ + H]⁺ (711.0999, 711.0991), [C₂₈H₁₇F₄IrN₄O₂ + Na]⁺ (733.0817, 733.0810). Elemental analysis (found, calculated) for C₂₈H₁₇F₄IrN₄O₂·1/2 H₂O, C (46.76, 46.79), H (2.48, 2.52), N (7.71, 7.80). Crystals were grown using vapor–vapor diffusion using CH₂Cl₂/acetone as the dissolving solvent and pentane as the precipitating solvent.

Compound 3, GP1: [(ppy)₂Ir(μ-Cl)]₂ (0.5012 g, 0.467 mmol), 5-methylpyrazine-2-carboxylic acid 4-oxide, Acipimox (0.2163 g, 1.403 mmol), K₂CO₃ (0.3887 g, 2.812 mmol), and acetone (42 mL) yielded 0.4285 g, 0.655 mmol, 70%. ¹H NMR (400 MHz, CDCl₃) δ 8.85 (s, 1H), 8.73 (ddd, J = 5.8, 1.6, 0.8 Hz, 1H), 7.89 (ddt, J = 12.2, 8.1, 1.2 Hz, 2H), 7.80–7.74 (m, 2H), 7.66–7.57 (m, 3H), 7.49 (t, J = 0.7 Hz, 1H), 7.20 (ddd, J = 7.3, 5.8, 1.4 Hz, 1H), 7.03 (ddd, J = 7.3, 5.8, 1.4 Hz, 1H), 6.95 (td, J = 7.5, 1.2 Hz, 1H), 6.88 (td, J = 7.5, 1.2 Hz, 1H), 6.82 (td, J = 7.4, 1.4 Hz, 1H), 6.76 (td, J = 7.4, 1.4 Hz, 1H), 6.38 (dd, J = 7.7, 1.2 Hz, 1H), 6.12 (dd, J = 7.7, 1.2 Hz, 1H), 2.31 (s, 3H). UV-Vis λ_{max} (ε M^{−1}cm^{−1}): 348 nm (11569), 396 (6311.4), 448 nm (2877.5). HRMS (found, calculated): [C₂₈H₂₁IrN₄O₃ + H]⁺ (655.1323, 655.1317), [C₂₈H₂₁IrN₄O₃ + Na]⁺ (677.1141, 677.1136). Elemental analysis (found, calculated) for C₂₈H₂₁IrN₄O₃·4/3 H₂O, C (49.59, 49.62), H (3.39, 3.52), N (8.11, 8.27). Crystals were grown using vapor–vapor diffusion using CH₂Cl₂ as the dissolving solvent and pentane as the precipitating solvent.

Compound 4, GP1: [(ppy)₂Ir(μ-Cl)]₂ (0.5001 g, 0.467 mmol), 5-methyl-2-pyrazinecarboxylic acid (0.1936 g, 1.402 mmol), K₂CO₃ (0.3870 g, 2.800 mmol), and acetone (40 mL) yielded 0.5193 g, 0.814 mmol, 87%. ¹H NMR (400 MHz, CDCl₃) δ 9.35 (d, J = 1.3 Hz, 1H), 8.73 (ddd, J = 5.8, 1.6, 0.8 Hz, 1H), 7.90 (dt, J = 8.2, 1.2 Hz, 1H), 7.86 (dt, J = 8.2, 1.2 Hz, 1H), 7.78–7.71 (m, 2H), 7.62 (dd, J = 7.7, 1.4 Hz, 1H), 7.59 (dd, J = 7.8, 1.4 Hz, 1H), 7.54 (dd, J = 1.3, 0.6 Hz, 1H), 7.46 (ddd, J = 5.8, 1.6, 0.7 Hz, 1H), 7.17 (ddd, J = 7.3, 5.8, 1.4 Hz, 1H), 7.01–6.91 (m, 2H), 6.87 (td, J = 7.5, 1.2 Hz, 1H), 6.82 (td, J = 7.4, 1.4 Hz, 1H), 6.76 (td, J = 7.4, 1.4 Hz, 1H), 6.39 (dd, J = 7.6, 1.2 Hz, 1H), 6.12 (dd, J = 7.6, 1.2 Hz, 1H), 2.50 (s, 3H). UV-Vis λ_{max} (ε M^{−1}cm^{−1}): 346 nm (9509.8), 393 nm (5335.3), 429 nm (3843.2). HRMS (found, calculated): [C₂₈H₂₁IrN₄O₂ + H]⁺ (639.1379, 639.1368), [C₂₈H₂₁IrN₄O₂ + Na]⁺ (661.1187, 661.1187). Elemental analysis (found, calculated) for C₂₈H₂₁IrN₄O₂·3/2 H₂O, C (50.66, 50.59), H (3.48, 3.64), N (8.32, 8.43). Crystals were grown using vapor–vapor diffusion using CH₂Cl₂ as the dissolving solvent and hexanes as the precipitating solvent.

Compound 5 was prepared according to a procedure reported in the literature (similar to **GP1**) and ^1H NMR data matched previously reported data for this compound; see Ref. [35]. Crystals were grown using vapor–vapor diffusion using CH_2Cl_2 as the dissolving solvent and hexanes as the precipitating solvent.

General procedure 2 (GP2) for the preparation of $[\text{Ir}(\text{C}^{\text{N}})_2(\text{N}^{\text{N}})]\text{PF}_6$ compounds (where $\text{C}^{\text{N}} = \text{ppy}$ or dfppy and $\text{N}^{\text{N}} =$ a 2,2'-bipyridine derivative) was adapted from methods previously reported in the literature; see Ref. [36]. $[(\text{C}^{\text{N}})_2\text{Ir}(\mu\text{-Cl})_2]$ and 2.2 equivalents of the appropriate N^{N} ligand were added to a dry flask with ethylene glycol (~10 mL). The heterogeneous mixture was heated to 150 °C under N_2 for 16–24 h. After cooling to room temperature, a saturated, aqueous solution of NH_4PF_6 (10 mL) was added to the resulting solution to precipitate the product. The precipitate was collected using vacuum filtration and washed with H_2O (3×15 mL) and Et_2O (3×15 mL), and the collected solid was dried in vacuo.

Compound 6, GP2: $[(\text{dfppy})_2\text{Ir}(\mu\text{-Cl})_2]$ (0.2432 g, 0.200 mmol), 2,2'-bipyrazine (0.0696 g, 0.440 mmol), and ethylene glycol (10 mL) yielded 0.3267 g, 0.373 mmol, 93%. ^1H NMR (400 MHz, DMSO-d_6) δ 10.26 (s, 2H), 8.91 (d, $J = 3.1$ Hz, 2H), 8.29 (d, $J = 8.5$ Hz, 2H), 8.06 (t, $J = 8.0$ Hz, 2H), 7.98 (d, $J = 3.1$ Hz, 2H), 7.82 (d, $J = 5.8$ Hz, 2H), 7.22 (t, $J = 6.8$ Hz, 2H), 7.02 (ddd, $J = 12.2, 9.4, 2.4$ Hz, 2H), 5.56 (dd, $J = 8.4, 2.4$ Hz, 2H). ^{19}F NMR (376 MHz, DMSO-d_6) δ -70 (d, $J = 710.75$ Hz, PF_6^-), -106 (dd, $J = 10.05, 19.19$ Hz, 2F), -108 (t, $J = 11.36$ Hz, 2F). ^{31}P NMR (162 MHz, DMSO-d_6) δ -144 ppm (sept, $J = 710.86$ Hz, PF_6^-). HRMS (found, calculated): $[\text{C}_{30}\text{H}_{18}\text{F}_{4\text{Ir}}\text{N}_6]^+$ (731.1162, 731.1154). Elemental analysis (found, calculated) for $\text{C}_{30}\text{H}_{20}\text{F}_{10}\text{IrN}_6\text{OP} \cdot \text{H}_2\text{O}$, C (40.67, 40.32), H (1.97, 2.26), N (9.21, 9.40). Crystals were grown using vapor–vapor diffusion using CH_2Cl_2 as the dissolving solvent and Et_2O as the precipitating solvent (plate-like crystals of **6·DCM**) or layering a solution of compound **6** in CH_2Cl_2 with Et_2O (tabular crystals of **6·0.5(DCM),0.5(Et₂O)**).

Compound 7, GP2: ^1H NMR data matched previously reported data for this compound [37]. Crystals were grown by layering a solution of compound **7** in CH_2Cl_2 with acetone followed by Et_2O .

Compound 8, GP2: ^1H NMR data matched previously reported data for this compound [38]. Crystals were grown using vapor–vapor diffusion using CH_2Cl_2 as the dissolving solvent and Et_2O as the precipitating solvent.

2.3. Single-Crystal X-ray Diffraction

Single-crystal X-ray diffraction data were collected at 100 K using a Bruker D8 Venture diffractometer. The data were collected using phi and omega scans (0.50° oscillations) with a Mo $\text{K}\alpha$ ($\lambda = 0.71073$ Å) microfocus source and Photon 2 detector. Data were processed (SAINT) and corrected for absorption using the multi-scan approach (SADABS), both within the Apex3 suite [39]. The structures were solved by intrinsic phasing and subsequently refined by full-matrix least squares on F^2 using the SHELXTL (2016/6) software package [40]. All non-hydrogen atoms were refined anisotropically. Hydrogen atoms attached to carbon atoms were refined in calculated positions using the appropriate riding models. Most of the complexes studied were found to crystallize as solvates: **1** with disordered THF, **2** with disordered CH_2Cl_2 and H_2O , **3** with CH_2Cl_2 , **4** with CH_2Cl_2 , **6** with CH_2Cl_2 or disordered CH_2Cl_2 and disordered Et_2O , and **7** with CH_2Cl_2 . Typical similarity restraints were employed to best model disordered solvent molecules having low site occupancy factors. Complete refinement details are summarized in Tables 1 and 2. CCDC 2335789–2335797 contain the supplementary crystallographic data for this paper and can be obtained from the Cambridge Crystallographic Data Centre.

Table 1. Crystallographic data for complexes 1–4.

	1- 1.25(THF)	2- 0.5(DCM),0.5(H ₂ O)	3- 2(DCM)	4- 2(DCM)
Formula	C ₃₃ H ₂₇ F ₄ IrN ₄ O _{4.25}	C _{28.5} H ₁₉ ClF ₄ IrN ₄ O _{2.5}	C ₃₀ H ₂₅ Cl ₄ IrN ₄ O ₃	C ₃₀ H ₂₅ Cl ₄ IrN ₄ O ₂
F. W. (g/mol)	815.78	761.13	823.54	807.54
Temperature (K)	100	100	100	100
Crystal system	triclinic	monoclinic	monoclinic	monoclinic
Space group	<i>P</i> -1	<i>P</i> ₂ / <i>c</i>	<i>P</i> ₂	<i>P</i> ₂
<i>a</i> (Å)	12.0056 (9)	20.1167 (11)	9.3656 (5)	9.3682 (6)
<i>b</i> (Å)	13.9227 (10)	16.8038 (10)	16.9853 (8)	16.9395 (10)
<i>c</i> (Å)	21.5251 (15)	17.1342 (9)	9.5139 (5)	9.4088 (5)
α (°)	84.548 (3)	90	90	90
β (°)	81.768 (3)	107.127 (2)	91.2046 (18)	91.347 (2)
γ (°)	87.722 (3)	90	90	90
Volume (Å ³)	3543.5 (4)	5535.1 (5)	1513.11 (13)	1492.69 (15)
Z	4	8	2	2
D(calcd) (g/cm ³)	1.529	1.827	1.808	1.797
μ , mm ⁻¹	3.829	4.984	4.804	4.866
F(000)	1600	2944	804	788
Cryst. Size (mm)	0.12 × 0.17 × 0.26	0.12 × 0.15 × 0.23	0.05 × 0.15 × 0.18	0.16 × 0.21 × 0.22
θ range, °	2.23 to 30.09	2.22 to 30.08	2.14 to 29.62	2.18 to 30.06
Reflns. collected	248152	137437	32766	33335
Indep. reflns.	20781	16232	8406	8622
R(int)	0.0388	0.0589	0.0374	0.0370
No. of parameters	904	794	381	372
No. of restraints	224	92	1	1
R indices (<i>I</i> > 2 σ (<i>I</i>))	R1 = 0.0362 wR2 = 0.1153	R1 = 0.0364 wR2 = 0.0778	R1 = 0.0204 wR2 = 0.0439	R1 = 0.0164 wR2 = 0.0376
R indices (all data)	R1 = 0.0409 wR2 = 0.1205	R1 = 0.0504 wR2 = 0.0872	R1 = 0.0236 wR2 = 0.0463	R1 = 0.0175 wR2 = 0.0396
S	1.109	1.111	1.038	0.946
Abs. struct. param. (Flack)	-	-	0.009(3)	0.015(3)
Largest diff. peak/hole (eÅ ⁻³)	2.623, -1.480	2.151, -2.036	1.495, -1.157	0.769, -0.699
CCDC dep. no.	2335789	2335790	2335791	2335792

Table 2. Crystallographic data for complexes 5–8.

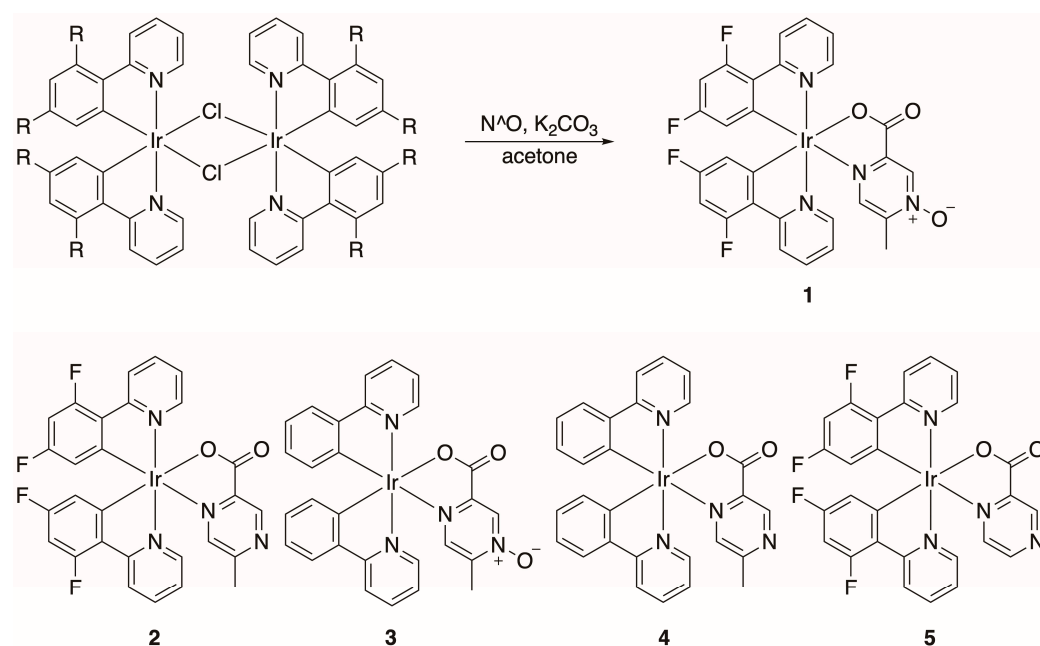
	5	6- (DCM)	6- 0.5(DCM), 0.5(Et ₂ O)	7- (DCM)	8
Formula	C ₂₇ H ₁₅ F ₄ IrN ₄ O ₂	C ₃₁ H ₂₀ Cl ₂ F ₁₀ IrN ₆ P	C _{32.5} H ₂₄ ClF ₁₀ IrN ₆ O _{0.5} P	C ₃₇ H ₃₂ Cl ₂ F ₁₀ IrN ₆ P	C ₃₀ H ₂₂ F ₆ IrN ₆ P
F. W. (g/mol)	695.63	960.60	955.20	1044.75	803.70
Temperature (K)	100	100	100	100	100
Crystal system	triclinic	monoclinic	triclinic	triclinic	orthorhombic
Space group	<i>P</i> -1	<i>P</i> ₂ / <i>c</i>	<i>P</i> -1	<i>P</i> -1	<i>Pbca</i>
<i>a</i> (Å)	8.8150 (6)	9.6985 (8)	13.8002 (6)	8.6227 (9)	10.8324 (4)
<i>b</i> (Å)	12.0339 (10)	24.7164 (18)	14.3504 (6)	13.5061 (13)	16.0987 (6)
<i>c</i> (Å)	22.3146 (17)	13.7261 (9)	17.3147 (8)	16.6738 (15)	31.5748 (10)
α (°)	87.528 (3)	90	72.193 (2)	104.272 (3)	90
β (°)	79.542 (3)	93.775 (3)	89.145 (2)	94.651 (4)	90
γ (°)	89.854 (3)	90	89.584 (2)	90.132 (4)	90
Volume (Å ³)	2325.6 (3)	3283.2 (4)	3264.3 (3)	1875.2 (3)	5506.3 (3)
Z	4	4	4	2	8
D(calcd) (g/cm ³)	1.987	1.943	1.944	1.850	1.939
μ , mm ⁻¹	5.808	4.370	4.316	3.834	4.983
F(000)	1336	1856	1856	1024	3120
Cryst. Size (mm)	0.08 × 0.08 × 0.12	0.03 × 0.11 × 0.17	0.06 × 0.12 × 0.20	0.08 × 0.26 × 0.28	0.06 × 0.12 × 0.14
θ range, °	2.35 to 26.50	2.10 to 25.50	2.10 to 25.50	2.24 to 27.94	2.36 to 26.00
Reflns. collected	81813	56722	68954	63741	53413
Indep. reflns.	9631	6099	12132	8981	5404
R(int)	0.0475	0.0468	0.0374	0.0401	0.0576
No. of parameters	685	460	982	518	397
No. of restraints	0	0	139	0	0
R indices (<i>I</i> > 2 σ (<i>I</i>))	R1 = 0.0214 wR2 = 0.0419	R1 = 0.0409 wR2 = 0.0865	R1 = 0.0404 wR2 = 0.0839	R1 = 0.0242 wR2 = 0.0561	R1 = 0.0319 wR2 = 0.0599
R indices (all data)	R1 = 0.0283 wR2 = 0.0464	R1 = 0.0498 wR2 = 0.0935	R1 = 0.0513 wR2 = 0.0944	R1 = 0.0274 wR2 = 0.0587	R1 = 0.0478 wR2 = 0.0707
S	1.191	1.067	1.100	1.123	1.219
Largest diff. peak/hole (eÅ ⁻³)	1.215, -0.938	1.811, -1.148	2.044, -1.501	1.534, -1.109	2.742, -1.650
CCDC dep. no.	2335793	2335794	2335795	2335796	2335797

3. Results and Discussion

3.1. Synthesis of Iridium(III) N-oxide Complexes

To generate N-oxide derivatives in which the N-oxide is not coordinated to the metal center, chlorobridged-Ir(III) dimers, [(dfppy)₂Ir(μ -Cl)]₂, and [(ppy)₂Ir(μ -Cl)]₂ were heated

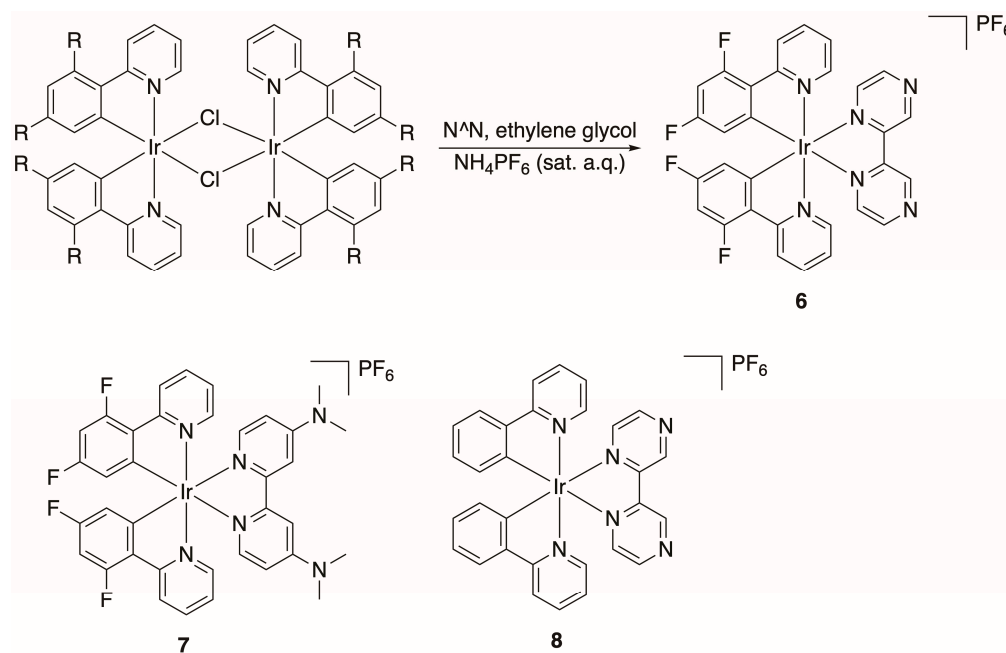
in the presence of 5-methylpyrazine-2-carboxylic acid 4-oxide (Acipimox) and K_2CO_3 using acetone as a solvent (Scheme 1), generating compound **1** and **3**. The same strategy was utilized to develop the non-*N*-oxide analogs, exploiting 5-methyl-2-pyrazinecarboxylic acid as the $N^{\wedge}O$ chelating ligand, generating compounds **2** and **4** (Scheme 1). This strategy resulted in no observable *N*-oxide metal coordination and the formation of one major product. The purity of all of these newly synthesized compounds was verified by elemental analysis, and their composition was supported by HRMS (Supporting Information, Figures S1–S5). Xing et al. also utilized the Acipimox ligand to generate Co(II) and Zn(II) coordination compounds and only observed one major species, where the selective coordination of the Acipimox ligand is due to the chelation effect imposed by the nitrogen and carboxylate formed in situ [33].



Scheme 1. Generation of neutral heteroleptic Ir(III) compounds containing *N*-oxides (**1** and **3**) and their non-*N*-oxide congeners (**2** and **4**). R = F or H and L = 5-methyl-2-pyrazinecarboxylic acid, Acipimox, or 2-pyrazinecarboxylic acid (for compound **5**).

Prior to exploiting *N*-oxide-containing ligands to append this functional group to Ir(III) compounds, we initially attempted to form the *N*-oxide by derivatizing synthesized Ir(III) species with uncoordinated nitrogen atoms. We envisioned oxidizing these nitrogen atoms with common oxidants often utilized to form *N*-oxides (e.g., mCPBA) [41]. Initial attempts have been unsuccessful; however, we are continuing to screen other oxidants for this strategy. Many of these species, such as compound **5** (Scheme 1) and compounds **6–8** (Scheme 2), have been previously synthesized but not characterized crystallographically.

The procedures to generate cationic Ir(III) compounds of the form $[Ir(C^{\wedge}N)_2(N^{\wedge}N)]PF_6$ (where $C^{\wedge}N = ppy$ or $dfppy$ and $N^{\wedge}N = a$ 2,2'-bipyridine derivative) exploited the cleavage of chlorobridged-Ir(III) dimers with neutral bidentate ligands (Scheme 2). For instance, heating $[(dfppy)_2Ir(\mu-Cl)]_2$ and 2,2'-bipyridine in ethylene glycol followed by the precipitation of the corresponding PF_6^- salt using NH_4PF_6 (sat. aq.) afforded the heteroleptic Ir(III) compound, **6**, which was verified by NMR, HRMS, and EA. Cationic compounds **7** and **8** have been previously reported in the literature, and we utilized 1H -NMR spectroscopy to initially verify product formation, which was later supported by full crystallographic characterization. Future efforts will focus on functionalizing the uncoordinated nitrogen atoms in these species to *N*-oxides (vide infra).



Scheme 2. Generation of cationic heteroleptic Ir(III) compounds for crystallographic characterization and to serve as precursors to *N*-oxides (R = F or H and L = 2,2'-bipyridine or 4,4'-di(dimethylamino)-2,2'-bipyridine).

$^1\text{H-NMR}$ spectra of compounds 1–8 contained many key features that are worth describing (Supporting Information, Figures S6–S10). In the previously reported cationic Ir(III) complexes (6–8), the innate symmetry of these molecules afforded nine (compound 6), ten (compound 7), and eleven (compound 8) ^1H -resonances. The presence of the 2-2'-bipyridine afforded many deshielded ^1H -resonances (~ 8 ppm) in compounds 6 and 8. For compound 7, the four equivalent homotopic methyl groups on the $-\text{NMe}_2$ groups served as a key feature at ~ 3 ppm. Likewise, in compounds 1–4, where all of the bidentate ligands surrounding the metal became inequivalent due to the asymmetry imposed by the *N*O chelating ligands, the methyl groups served as a valuable spectroscopic handle. In compounds 1–4, the methyl group on the 2-pyrazinecarboxylic acid portion of the molecule provided distinct resonances at 2.34 ppm (compound 1), 2.58 ppm (compound 2), 2.31 ppm (compound 3), and 2.50 ppm (compound 4). Even prior to structural validation from X-ray data, this indicated that only one major product had been synthesized in each case.

3.2. Structural Comparison of Iridium(III) *N*-oxide Complexes with Comparable Iridium(III) Complexes with Non-oxidized Ligands, 1–4

In all four complexes, iridium is a six-coordinate metal center, coordinating two atoms from each ligand and accumulating to the $[\text{Ir}(\text{C}_2\text{N}_3\text{O})]$ coordination (Figure 2). The bidentate coordination of the 5mpcaO and 5mpca ligands in all four complexes occurs through one of the carboxylate oxygen atoms and its nearest nitrogen atom, leaving the *N*-oxide (in 1 and 3) or its corresponding bare nitrogen atom (in 2 and 4) exposed. Each of the ligands is monoanionic, stabilizing the Ir(III) oxidation state. In 1 and 2, the asymmetric units consist of two unique Ir(III) complexes as well as disordered THF and CH_2Cl_2 molecules, respectively. In 3 and 4, the asymmetric units contain only one unique Ir(III) complex and two well-ordered CH_2Cl_2 molecules.

The six-coordinate Ir(III) in each complex is a distorted octahedron (Table 3). The angular distortion is similar for all of the octahedra, with complex 1 exhibiting the extremes of the *trans*-angles for the series, ranging from $169.52(14)^\circ$ to $175.83(13)^\circ$. The complexes also all show a significant *trans*-effect in the Ir–O and Ir–N bond lengths for the 5mpcaO and 5mpca ligands, whose oxygen and nitrogen atoms occur opposite the coordinated carbon atoms of the difluorophenylpyridine (dfppy) and phenylpyridine (ppy) ligands.

The *trans*-effects of similar magnitudes are observed in other iridium complexes of dfppy and ppy [42–44]. The N–O distances in **1** and **3** are similar to those of the Co(II) and Zn(II) complexes with 5mpcaO, [Co(5mpcaO)₂(H₂O)₂] \cdot 2H₂O and [Zn(5mpcaO)₂(H₂O)₂] \cdot 2H₂O, respectively, which are to our knowledge the only other metal complexes of 5mpcaO to be characterized crystallographically [33]. These distances are on the shorter end of the N–O bond lengths surveyed in the literature for molecular *N*-oxide crystals [45], indicating some contribution of the N⁺=O resonance form in the Ir(III)-complexed ligand (Supporting Information, Figure S11). Complexes such as **2** and **4** involving the non-oxidized 5mpca ligand are somewhat more common in the structural literature, including one iridium complex of 5mpca and two 3,5-bis(trifluoromethyl)phenyl ligands [46]. A similar *trans*-influence to that found in **2** and **4** affecting the Ir–O and Ir–N bond lengths is observed in that structure.

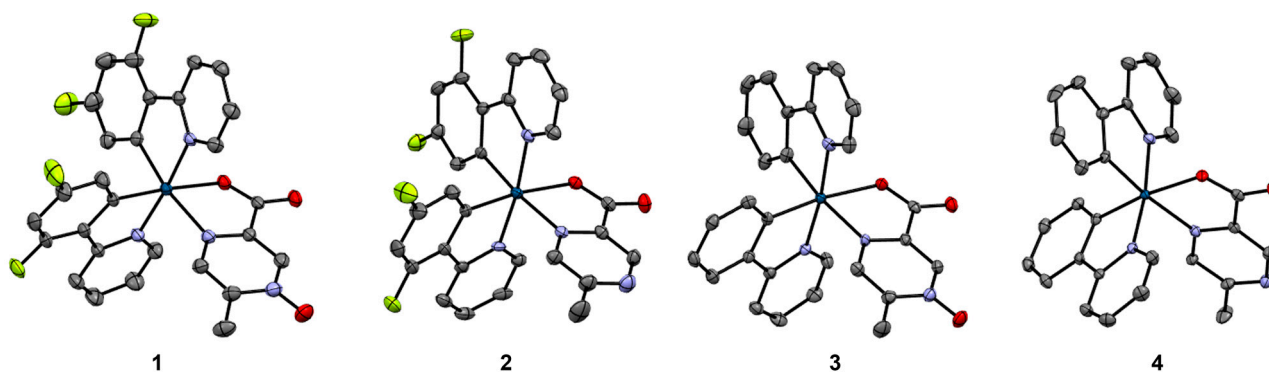


Figure 2. Crystal structure of complexes **1–4**, shown as 50% probability ellipsoids. Iridium atoms are dark blue, carbon atoms are gray, nitrogen atoms are purple, oxygen atoms are red, and fluorine atoms are lime green. Hydrogen atoms and solvent molecules are omitted for clarity. For complexes **1** and **2**, where two similar but crystallographically unique complexes occur in the asymmetric unit, only one complex is shown as a representative example.

Table 3. Selected interatomic distances (Å) and angles (°) in **1–4**.

Bond	1	2	3	4																																																														
Ir–O	2.151 (3)	2.150 (3)	2.177 (2)	2.1699 (18)																																																														
	2.156 (3)	2.155 (3)			Ir–N	2.141 (3)	2.114 (4)	2.138 (3)	2.136 (3)	2.126 (4)	2.131 (4)	Ir–N _{dfppy/ppy}	2.039 (3)	2.021 (3)	2.040 (3)	2.036 (3)	2.043 (3)	2.052 (3)	2.040 (4)	2.045 (4)	2.052 (4)	2.048 (3)	Ir–C _{dfppy/ppy} (<i>trans</i> O)	2.045 (4)	2.045 (4)	1.995 (4)	1.994 (3)	1.993 (4)	1.991 (4)	Ir–C _{dfppy/ppy} (<i>trans</i> N)	1.987 (5)	1.996 (4)	1.999 (4)	2.002 (3)	2.001 (4)	2.002 (4)	N–O	2.003 (5)	1.999 (4)	1.283 (5)	-	1.283 (5)	-	O–Ir–C (<i>trans</i>)	1.279 (8)	-	172.6 (2)	172.89 (16)	175.83 (13)	172.18 (14)	N–Ir–C (<i>trans</i>)	175.17 (16)	174.21 (14)	171.52 (15)	171.32 (12)	169.52 (14)	172.54 (14)	N–Ir–N (<i>trans</i>)	170.8 (2)	175.37 (16)	173.45 (13)	172.40 (11)	174.92 (13)	172.85 (15)		172.29 (16)
Ir–N	2.141 (3)	2.114 (4)	2.138 (3)	2.136 (3)																																																														
	2.126 (4)	2.131 (4)			Ir–N _{dfppy/ppy}	2.039 (3)	2.021 (3)	2.040 (3)	2.036 (3)	2.043 (3)	2.052 (3)		2.040 (4)	2.045 (4)			2.052 (4)	2.048 (3)	Ir–C _{dfppy/ppy} (<i>trans</i> O)	2.045 (4)	2.045 (4)	1.995 (4)	1.994 (3)	1.993 (4)	1.991 (4)	Ir–C _{dfppy/ppy} (<i>trans</i> N)	1.987 (5)	1.996 (4)	1.999 (4)	2.002 (3)	2.001 (4)	2.002 (4)	N–O	2.003 (5)	1.999 (4)	1.283 (5)	-	1.283 (5)	-	O–Ir–C (<i>trans</i>)	1.279 (8)	-	172.6 (2)	172.89 (16)	175.83 (13)	172.18 (14)	N–Ir–C (<i>trans</i>)	175.17 (16)	174.21 (14)	171.52 (15)	171.32 (12)	169.52 (14)	172.54 (14)	N–Ir–N (<i>trans</i>)	170.8 (2)	175.37 (16)	173.45 (13)	172.40 (11)	174.92 (13)	172.85 (15)		172.29 (16)	174.90 (14)			
Ir–N _{dfppy/ppy}	2.039 (3)	2.021 (3)	2.040 (3)	2.036 (3)																																																														
	2.043 (3)	2.052 (3)																																																																
	2.040 (4)	2.045 (4)			2.052 (4)	2.048 (3)																																																												
Ir–C _{dfppy/ppy} (<i>trans</i> O)	2.045 (4)	2.045 (4)	1.995 (4)	1.994 (3)																																																														
	1.993 (4)	1.991 (4)																																																																
Ir–C _{dfppy/ppy} (<i>trans</i> N)	1.987 (5)	1.996 (4)	1.999 (4)	2.002 (3)																																																														
	2.001 (4)	2.002 (4)																																																																
N–O	2.003 (5)	1.999 (4)	1.283 (5)	-																																																														
	1.283 (5)	-																																																																
O–Ir–C (<i>trans</i>)	1.279 (8)	-	172.6 (2)	172.89 (16)																																																														
	175.83 (13)	172.18 (14)																																																																
N–Ir–C (<i>trans</i>)	175.17 (16)	174.21 (14)	171.52 (15)	171.32 (12)																																																														
	169.52 (14)	172.54 (14)																																																																
N–Ir–N (<i>trans</i>)	170.8 (2)	175.37 (16)	173.45 (13)	172.40 (11)																																																														
	174.92 (13)	172.85 (15)																																																																
	172.29 (16)	174.90 (14)																																																																

The exposure of the *N*-oxide or its corresponding bare nitrogen atom on the outside of the complex is influential in establishing the intermolecular interactions and packing patterns that are observed in **1–4**. In **1**, the *N*-oxide oxygen atoms maintain short O \cdots π

contacts between symmetry-equivalent complexes to form dimers, which then associate through C-H \cdots O interactions with the *N*-oxide oxygen atoms of the second unique complex (Figure 3). An offset $\pi\cdots\pi$ stacking interaction further stabilizes the central dimer. The resulting clusters then assemble into a three-dimensional network via additional C-H \cdots O_{carboxylate} interactions. The space between the complexes in **1** is occupied by disordered THF molecules (Supporting Information, Figure S12). In **2**, the bare nitrogen atom of the 5mpca ligand of one of the unique complexes acts as an acceptor for a C-H \cdots N interaction originating from the second unique complex (Figure 3), with the interaction connecting neighboring complexes along [1 0 -1]. The bare nitrogen atom of this second complex, however, does not maintain any short intermolecular contact with neighboring complexes. Additional C-H \cdots O_{carboxylate}, C-H \cdots F, and $\pi\cdots\pi$ interactions further extend the packing structure to three dimensions, where voids are occupied by water molecules and disordered CH₂Cl₂ molecules (Supporting Information, Figure S13). The water molecules facilitate hydrogen bonding interactions that bridge the uncoordinated carboxylate oxygen atoms of neighboring complexes along the *a*-axis.

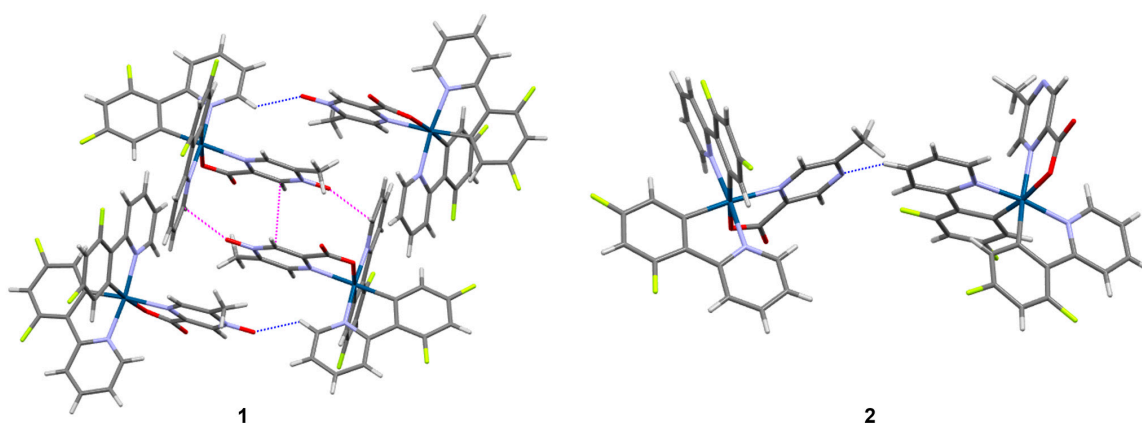


Figure 3. Intermolecular interactions involving the *N*-oxide and bare nitrogen atoms of complexes **1** and **2**. C-H \cdots O and C-H \cdots N interactions are shown as dashed blue lines, while O $\cdots\pi$ and $\pi\cdots\pi$ interactions are shown as dashed magenta lines to the nearest carbon atom. Iridium atoms are dark blue, carbon atoms are gray, nitrogen atoms are purple, oxygen atoms are red, fluorine atoms are lime green, and hydrogen atoms are white.

Complexes **3** and **4** crystallized with an identical solvent content of two CH₂Cl₂ molecules per complex. Despite their similar compositions, space groups, and unit cell parameters (the unit cell volume of **3** is only about 1.4% larger than that of the non-oxidized **4**), subtle perturbations are observed in the packing structure exerted by the oxygen atom in **3** compared to the bare nitrogen atom in **4**. The *N*-oxide in **3** acts as a C-H \cdots O acceptor for two neighboring complexes and a Cl \cdots O halogen bond acceptor (Cl \cdots O = 2.963(6) Å, normalized halogen bond length = 0.89) for one of the CH₂Cl₂ molecules (Figure 4). The C-H \cdots O interactions, in particular, extend the intermolecular motif into a two-dimensional sheet parallel to (1 0 1). Additional C-H \cdots O_{carboxylate} and C-H $\cdots\pi$ interactions further extend the long-range structure to three dimensions, accommodating the additional CH₂Cl₂ molecules (Supporting Information, Figure S14). Complex **4** appears to adopt the opposite relative chirality in space group *P*2₁, and there are subtle positional differences of neighboring molecules compared to **3** that favor C-H $\cdots\pi$ interactions since the equivalent C-H \cdots O interactions to the *N*-oxide in **3** are no longer operable in **4** (Figure 4). An equivalent C-H \cdots N interaction to the bare nitrogen atom does not appear to be enabled. Likewise, the nearest CH₂Cl₂ molecule is arranged toward a Cl $\cdots\pi$ interaction rather than Cl \cdots N (even though nitrogen is typically a good halogen bond acceptor) now that the Cl \cdots O interaction is removed. The packing is extended into three dimensions by the continuation of the numerous C-H $\cdots\pi$ interactions as well as C-H \cdots O_{carboxylate} interactions, again accommodating the cocrystallized CH₂Cl₂ molecules (Supporting Information, Figure S15).

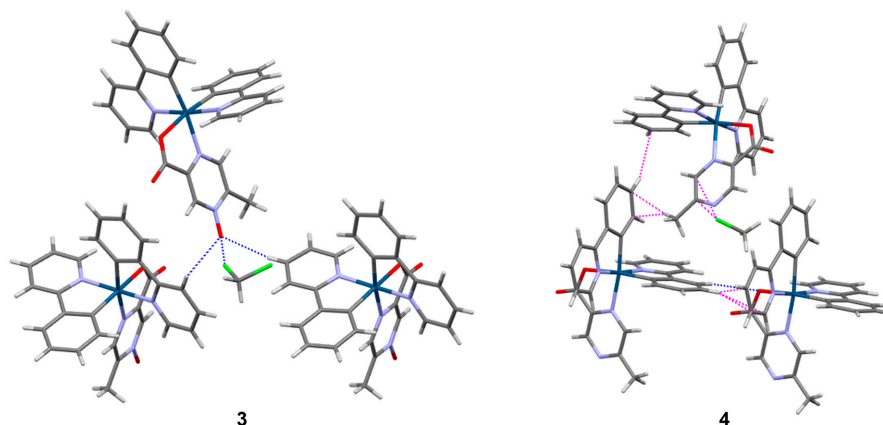


Figure 4. Selected intermolecular interactions in complexes **3** and **4**. C-H...O, C-H...N, and Cl...O interactions are shown as dashed blue lines, while C-H... π and Cl... π interactions are shown as dashed magenta lines to the nearest carbon atom. Iridium atoms are dark blue, carbon atoms are gray, nitrogen atoms are purple, oxygen atoms are red, chlorine atoms are green, and hydrogen atoms are white.

3.3. Electronic Characterization of 1–4

To better understand the electronics of compounds **1–4**, the cyclic voltammograms of each species were obtained (Figure 5). Based on literature precedent, we assigned the features at positive potentials to an Ir^{III}/Ir^{IV} oxidation [47]. The potentials of these features depend on what cyclometallating ligand was utilized. For instance, when the electron-deficient 2-(2',4'-difluorophenyl)pyridine is used as a cyclometallating ligand, the metal center's oxidation occurs at a more positive potential (e.g., compound **1**) as compared to when phenylpyridine is used as a cyclometallating ligand (e.g., compound **3**). The reversible anodic features appearing between -1.84 and -2.00 V were assigned to the reduction of the pyrazinecarboxylic acid ligands based on literature precedent [48]. In compounds **1** and **3**, the presence of an *N*-oxide anodically shifts the reduction potential. For instance, in comparing compounds **1** and **2**, the reversible reduction feature occurs at -1.84 and -1.99 V, respectively. Based on electrochemical data, this suggests that the *N*-oxide is acting as an electron-withdrawing group. This is of importance because although the oxygen is inductively withdrawing, it can act as an electron-donating group based on resonance (Figure S11).

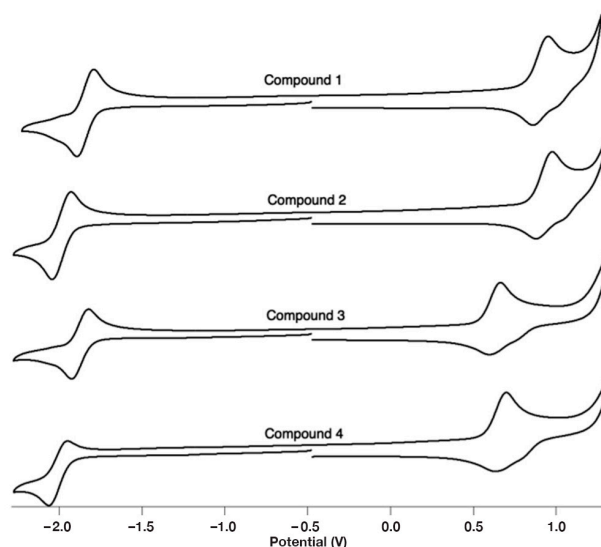


Figure 5. Cyclic voltammograms of compounds **1–4**. Conditions: [Ir]~1 mM in CH₂Cl₂ (0.1 M TBAPF₆), glassy carbon working electrode, Ag/Ag⁺ reference electrode. The *x*-axis reports voltages vs. ferrocene (FcH) as determined by running a voltammogram of FcH before and after data collection.

3.4. Structural Characterization of Iridium(III) Complexes with Additional Exposed Nitrogen Atoms 5–8

The Ir(III) complexes 5–8 adopt similar six-coordinate environments to those in 1–4 (Figure 6). Each is coordinated in a bidentate fashion by three ligands. The dfppy ligands of 5–7, the ppy ligands of 8, and the pyrazine carboxylic acid ligand of 5 are all monoanionic, while the bipyrazine (bpz) ligands of 6 and 8 and the di(dimethylamino)-2,2'-bipyridine ligand of 7 are neutral. In this way, the resulting complexes with Ir(III) are neutral in the case of 5 and monocationic in the case of 6–8. Complexes 6–8 therefore crystallize as $[\text{PF}_6]^-$ salts. Furthermore, complex 6 was obtained as two different solvates having two slightly different solvent contents that resulted in packing differences. All the complexes exhibit a *trans*-lengthening effect for Ir–N (and Ir–O in the case of 5) bonds that are *trans* to the Ir–C bonds to dfppy or ppy ligands (Table 4).

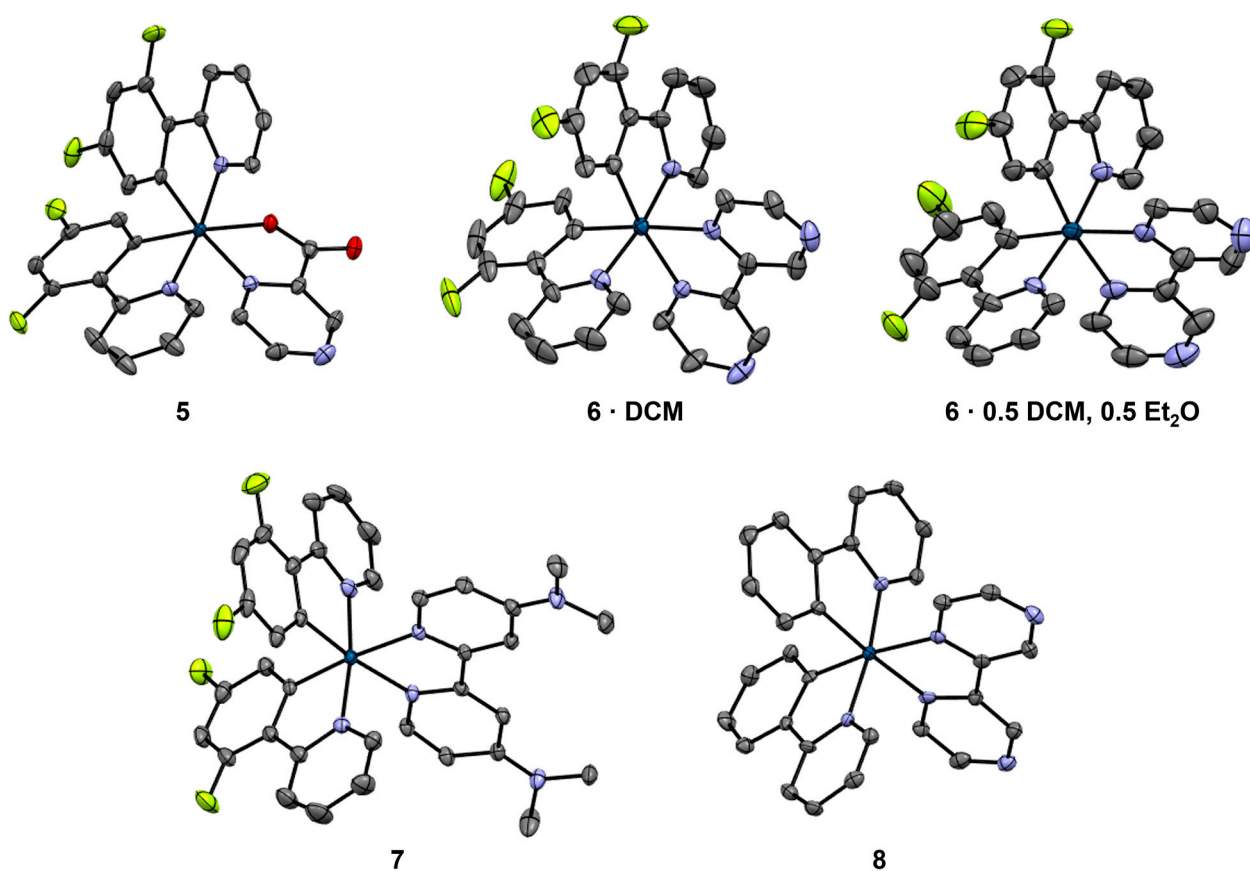


Figure 6. Crystal structure of complexes 5–8, shown as 50% probability ellipsoids. Iridium atoms are dark blue, carbon atoms are gray, nitrogen atoms are purple, oxygen atoms are red, and fluorine atoms are lime green. Hydrogen atoms and solvent molecules are omitted for clarity. Two renderings are given for complex 6, derived from the two different solvate crystal structures obtained for 6. For complexes 5 and 6·0.5(DCM),0.5(Et₂O), where two similar but crystallographically unique complexes occur in the asymmetric unit, only one complex is shown as a representative example.

The pyrazine-2-carboxylate ligand of 5 is fairly common among mixed-ligand metal coordination chemistry, including the full structural characterization of cyclometallated Ir(III) complexes with 2-(3-phenylquinoxalin-2-yl)phenyl [49], 2-(1,3-benzoxazol-2-yl)phenyl [50], 9-(pyridine-2-yl)-9H-carbazol-1-yl [51], and 3,5-difluoro-2-(4-methylpyridin-2-yl)phenyl ligands [52]. Complexes in 5 assemble in chains via cooperative C–H···O, C–H···N, C–H··· π , and π ··· π interactions involving two crystallographically unique complexes (Figure 7). At the center of this chain is an offset π ··· π stacking interaction between the pyrazine regions of symmetry-equivalent Ir₂ complexes (plane-to-plane distance of 3.29 Å) similar to that

observed in the bis(3,5-difluoro-2-(4-methylpyridin-2-yl)phenyl)-pyrazine-2-carboxylato)-Ir(III) complex [52]. The exposed nitrogen atom of the pyrazine region of the second unique complex, Ir1, forms the C-H \cdots N interaction with the Ir2 complex. An offset π overlap between dfppy ligands of neighboring Ir1 complexes is also prevalent. Additionally, complementary C-H \cdots O, C-H \cdots F, and C-H \cdots π interactions extend the long-range packing to three dimensions (Supporting Information, Figure S16).

Table 4. Selected interatomic distances (Å) and angles (°) in 5–8.

Bond	5	6 (DCM)	6 0.5(DCM),0.5(Et ₂ O)	7	8
Ir-O	2.154 (2) 2.155 (2)	-	-	-	-
Ir-N	2.138 (3) 2.136 (3)	2.132 (5) 2.133 (5)	2.112 (5) 2.125 (5) 2.125 (5) 2.126 (5)	2.131 (2) 2.135 (2)	2.135 (4) 2.141 (4)
Ir-N _{dfppy/ppy}	2.023 (3) 2.047 (3) 2.030 (3) 2.041 (4)	2.046 (5) 2.047 (5)	2.054 (5) 2.057 (5) 2.048 (6) 2.053 (6)	2.034 (3) 2.037 (2)	2.052 (4) 2.052 (4)
Ir-C _{dfppy/ppy}	1.993 (3) 2.012 (3) 1.995 (3) 2.002 (4)	1.998 (7) 2.012 (7)	1.998 (7) 2.028 (6) 2.012 (6) 2.016 (6)	2.016 (3) 2.016 (3)	2.016 (6) 2.022 (5)
O-Ir-C (<i>trans</i>)	174.81 (12) 173.78 (12)	-	-	-	-
N-Ir-C (<i>trans</i>)	171.94 (11) 172.56 (12)	171.1 (2) 175.6 (2)	172.6 (2) 170.8 (2) 172.4 (2) 175.4 (2)	171.25 (10) 174.75 (10)	172.37 (17) 175.70 (19)
N-Ir-N (<i>trans</i>)	172.12 (11) 173.16 (12)	171.6 (2)	173.3 (2) 172.9 (2)	171.97 (10)	172.81 (16)

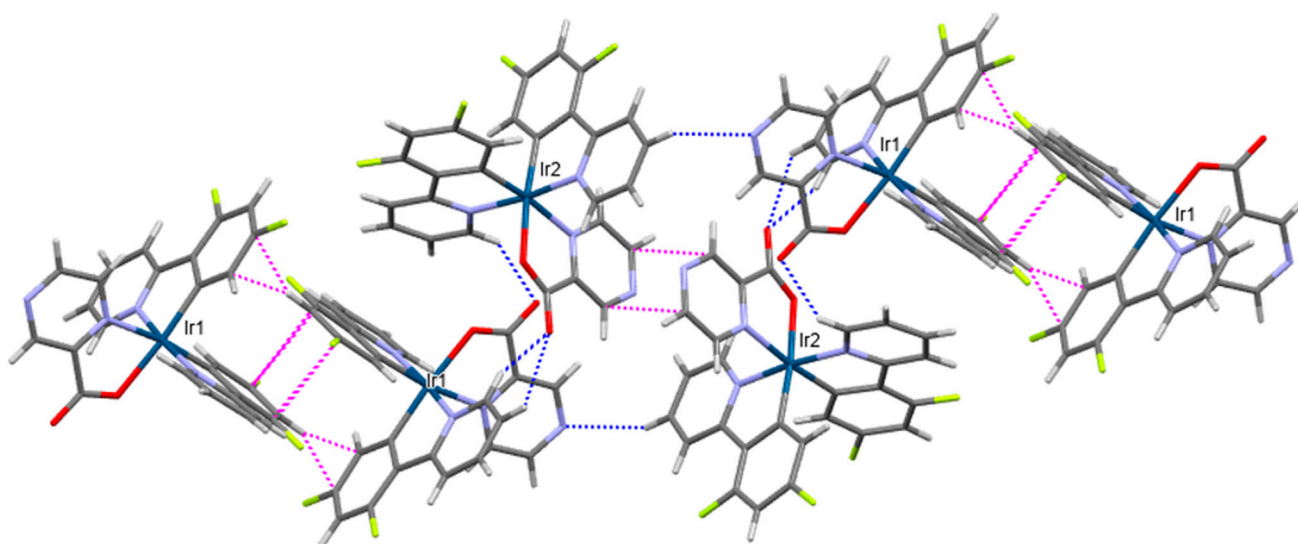


Figure 7. Intermolecular interactions involving the formation of chains in 5. C-H \cdots O and C-H \cdots N interactions are shown as dashed blue lines, while C-H \cdots π and π \cdots π interactions are shown as dashed magenta lines to the nearest carbon atom. Iridium atoms are dark blue, carbon atoms are gray, nitrogen atoms are purple, oxygen atoms are red, fluorine atoms are lime green, and hydrogen atoms are white.

In **6**·(DCM), complexes form dimers through C-H···N interactions involving one of the dfppy ligands of one complex and one of the external nitrogen atoms of the bpz ligands of a neighboring complex (Figure 8). Numerous short C-H···F interactions to the [PF₆][−] anions, C-H···Cl interactions to the CH₂Cl₂ solvent molecules, and C-F···π contacts between neighboring complexes complete the three-dimensional packing network (Supporting Information, Figure S17). In **6**·0.5(DCM),0.5(Et₂O), a similar dimeric coupling of complexes via C-H···N occurs between symmetry-equivalent Ir1 complexes (Figure 8). In this case, the second unique complex, Ir2, appends to these dimers via C-H···N, where the accepting nitrogen atom is the second external nitrogen atom on the bpz ligand of Ir1. In this way, both nitrogen atoms of the bpz ligand of Ir1 are involved in intermolecular short contacts, while neither of the nitrogen atoms of the bpz ligand of Ir2 feature short contacts. The result is a finite four-complex chain. Numerous other short contacts (C-H···O, C-H···F, C-H···Cl, and C-H···π) to neighboring finite chains, [PF₆][−] anions, and solvent molecules extend the packing structure (Supporting Information, Figure S18). By comparison, only one cyclometallated Ir(III) complex involving a bpz ligand has been reported with full crystallographic characterization, that of (2,2′-bipyrazine)-bis(2-pyridin-2-yl)-4,6-bis(trifluoromethyl)phenyl-iridium hexafluorophosphate [53]. Neighboring complexes in that structure do not form C-H···N dimers but rather form continuous chains of C-H···N interactions. That behavior is more similar to what is observed in **8**, where C-H···N interactions form chains along the *a*-axis (Figure 8). Neighboring chains are then related primarily through C-H···π interactions or the [PF₆][−] anion via C-H···F contacts, facilitating the long-range packing (Supporting Information, Figure S20). We would note that the differing solvent content in **6**·(DCM) versus **6**·0.5(DCM),0.5(Et₂O) led to significant packing differences and long-range interactions in these structures. This likely occurs since the DCM and Et₂O solvent molecules do not overlap with each other (as they might be if **6**·(DCM) and **6**·0.5(DCM),0.5(Et₂O) were isostructural) but instead occupy unique sites in the lattice. Et₂O is disordered over two orientations in **6**·0.5(DCM),0.5(Et₂O), but these orientations overlap with one another with a unity sum rather than disordered with DCM, which is fully ordered in its own position. The 0.5(DCM) and 0.5(Et₂O) solvent content thus results from the occurrence of two unique Ir(III) complexes in the asymmetric unit, one unique DCM molecule, and two half-occupied overlapping Et₂O molecules. We postulate that Et₂O was able to be introduced in the crystals of **6**·0.5(DCM),0.5(Et₂O) because of the locally higher Et₂O concentrations present at the solvent interface in the solvent-layering experiment compared to the vapor diffusion experiment that produced **6**·(DCM).

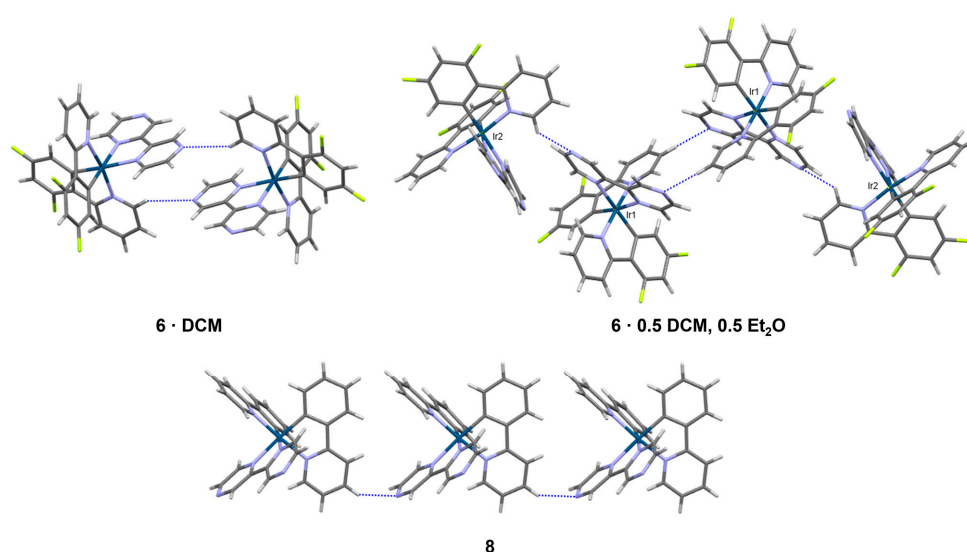


Figure 8. Selected intermolecular interactions involving the bipyrazine nitrogen atoms in **6** and **8**. C-H···N interactions are shown as dashed blue lines. Iridium atoms are dark blue, carbon atoms are gray, nitrogen atoms are purple, fluorine atoms are lime green, and hydrogen atoms are white.

The crystal structures of four cyclometallated Ir(III) complexes involving the 4,4'-di(dimethylamino)-2,2'-bipyridine ligand are reported in the literature, in complexes having the additional 2-pyridin-2-ylthien-3-yl [54], 5-formyl-2-(pyridin-2-yl)phenyl [55], 3,5-difluoro-2-(1H-pyrazol-1-yl)phenyl [56], or 3,5-difluoro-2-(2-methyl-2H-tetrazol-5-yl)phenyl ligands [57]. Since the external nitrogen atoms of the 4,4'-di(dimethylamino)-2,2'-bipyridine ligand are occupied by methyl groups, the packing structure of **7** is generated through a complex network of $\pi \cdots \pi$ and C-H $\cdots\pi$ interactions (Figure 9). The voids between the bulky complexes are occupied by CH₂Cl₂ molecules and [PF₆][−] anions, which facilitate additional C-H \cdots Cl and C-H \cdots F interactions to further stabilize the structure (Supporting Information, Figure S19).

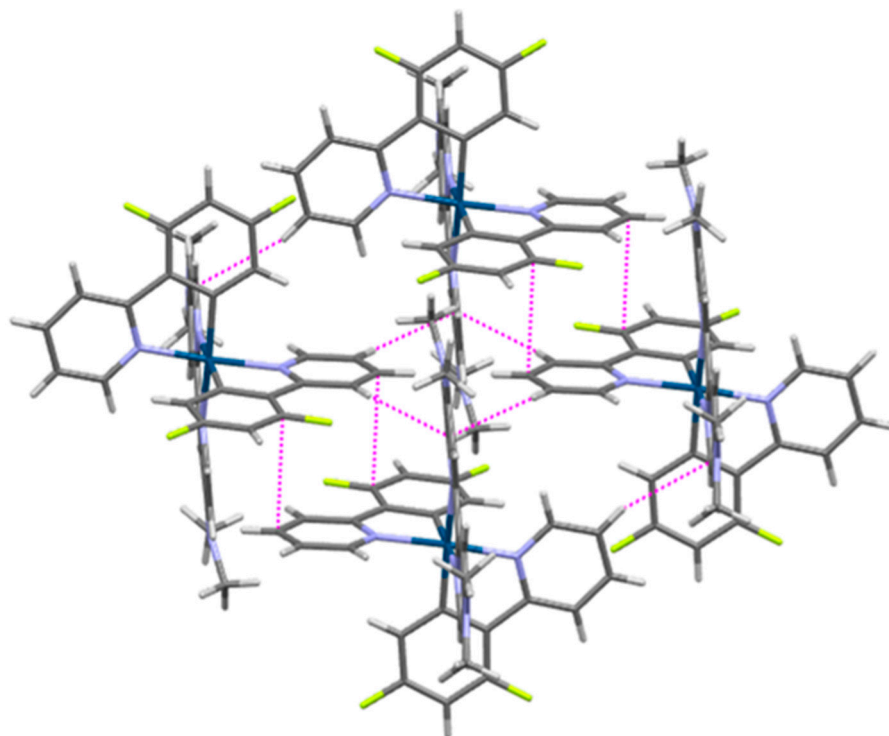


Figure 9. Selected intermolecular interactions in **7**. C-H $\cdots\pi$ and $\pi \cdots \pi$ interactions are shown as dashed magenta lines to the nearest carbon atom. Iridium atoms are dark blue, carbon atoms are grey, nitrogen atoms are purple, fluorine atoms are lime green, and hydrogen atoms are white.

4. Conclusions

We synthesized and characterized two rare examples of cyclometallated Ir(III) compounds containing the *N*-oxide functional group, where the *N*-oxide is not coordinated to the metal center. Electrochemical analysis results indicate that the *N*-oxide functional group acts as an electron-withdrawing group. Single-crystal X-ray diffraction analysis confirmed the ligand coordination and the exposed *N*-oxide group. The *N*-oxides enabled significant C-H \cdots O and O $\cdots\pi$ interactions between neighboring complexes that distinguished the packing structures from the non-oxidized congeners. Moreover, the X-ray analysis results of several additional species, having exposed nitrogen atoms not coordinated to the Ir(III) center, are reported. The single-crystal analysis of these species indicated the prevalence of C-H \cdots N interactions in combination with $\pi \cdots \pi$ and C-H $\cdots\pi$ interactions. A distinguishing feature in some of these structures is the formation of C-H \cdots N dimers or finite chains versus infinite chains of C-H \cdots N interactions. These species all contain uncoordinated nitrogen atoms, and our group is working to develop synthetic methodologies to oxidize these species to their corresponding *N*-oxide analogs using traditional methods commonly utilized in organic synthesis (e.g., *m*CPBA) [41]. Although the *N*-oxide functional group has been incorporated into various organic motifs and has shown utility in various applications [1–5], including imaging hypoxia in tumor cells [3–5], there are limited examples of

N-oxide-containing transition metal compounds where the *N*-oxide is uncoordinated to the metal center. By comparing two novel examples of transition metal *N*-oxides to their non-*N*-oxide congeners, we were able to determine how this functional group impacts the structural and electrochemical properties of heteroleptic Ir(III) species.

Supplementary Materials: The following supporting information can be downloaded at: <https://www.mdpi.com/article/10.3390/cryst14030281/s1>, Figures S1–S6: HRMS spectra; Figures S7–S10: ¹H-NMR spectra; Figure S11: *N*-oxide resonance; Figures S12–S20: crystallographic packing diagrams.

Author Contributions: Conceptualization, E.E.S. and J.A.P.; methodology, E.E.S., C.D.M. and J.A.P.; validation, E.E.S., C.D.M. and J.A.P.; formal analysis, C.D.M., J.A.P. and E.E.S.; investigation, C.D.M., J.A.P., E.E.S., E.K.H., M.W. and D.A.T.; writing—original draft preparation, C.D.M., J.A.P. and E.E.S.; writing—review and editing, C.D.M., J.A.P. and E.E.S.; visualization, C.D.M., J.A.P. and E.K.H.; funding acquisition, J.A.P. and E.E.S. All authors have read and agreed to the published version of the manuscript.

Funding: Internal funding from the University of Tennessee at Chattanooga supported this research: Faculty Development Grant, Research and Creative Activity Grant, and a SEARCH Award (from the Office for Undergraduate Research and Creative Endeavor).

Data Availability Statement: CCDC 2335789-2335797 contain the supplementary crystallographic data for this paper. These data can be obtained from the CCDC, 12 Union Road, Cambridge CB2 1EZ, UK; Fax: +44 1223 336033.

Acknowledgments: HRMS measurements were obtained by David Blauch at Davidson College using an Agilent LC-MS acquired through an NSF MRI award (CHE-1624377). The authors would like to thank Madelyn R. Shevlin, Luke L. Hair, and India I. Toth for assisting in the validation of synthetic procedures.

Conflicts of Interest: The authors declare no conflicts of interest. The funders had no role in the design of the study; in the collection, analyses, or interpretation of data; in the writing of the manuscript; or in the decision to publish the results.

References

1. Bull, J.A.; Mousseau, J.J.; Pelletier, G.; Charette, A.B. Synthesis of Pyridine and Dihydropyridine Derivatives by Regio- and Stereoselective Addition to *N*-Activated Pyridines. *Chem. Rev.* **2012**, *112*, 2642–2713. [CrossRef]
2. Mfuh, A.M.; Larionov, O.V. Heterocyclic *N*-Oxides—An Emerging Class of Therapeutic Agents. *Curr. Med. Chem.* **2015**, *22*, 2819–2857. [CrossRef]
3. Kang, D.; Cheung, S.T.; Wong-Rolle, A.; Kim, J. Enamine *N*-Oxides: Synthesis and Application to Hypoxia-Responsive Prodrugs and Imaging Agents. *ACS Cent. Sci.* **2021**, *7*, 631–640. [CrossRef] [PubMed]
4. Knox, H.J.; Hedhli, J.; Kim, T.W.; Khalili, K.; Dobrucki, L.W.; Chan, J. A bioreducible *N*-oxide-based probe for photoacoustic imaging of hypoxia. *Nat. Commun.* **2017**, *8*, 1794. [CrossRef]
5. Knox, H.J.; Kim, T.W.; Zhu, Z.; Chan, J. Photophysical Tuning of *N*-Oxide-Based Probes Enables Ratiometric Photoacoustic Imaging of Tumor Hypoxia. *ACS Chem. Biol.* **2018**, *13*, 1838–1843. [CrossRef]
6. Delahoussaye, Y.M.; Evans, J.W.; Brown, J.M. Metabolism of tirapazamine by multiple reductases in the nucleus. Abbreviations: TPZ, tirapazamine; P450 reductase, NADPH:cytochrome P450 reductase; PMSF, phenylmethylsulfonyl fluoride; DTT, dithiothreitol; DHR123, dihydrorhodamine 123; DAPI, 4',6-diamidino-2-phenylindole, dihydrochloride; SN, supernatant from nuclei; LS, low salt; HS, high salt; and NM, nuclear matrix. *Biochem. Pharmacol.* **2001**, *62*, 1201–1209. [CrossRef]
7. Skerritt, J.H.; Johnston, G.A. Enhancement of GABA binding by benzodiazepines and related anxiolytics. *Eur. J. Pharmacol.* **1983**, *89*, 193–198. [CrossRef]
8. Lo, K.K.-W. Luminescent Rhenium(I) and Iridium(III) Polypyridine Complexes as Biological Probes, Imaging Reagents, and Photocytotoxic Agents. *Acc. Chem. Res.* **2015**, *48*, 2985–2995. [CrossRef] [PubMed]
9. Baggaley, E.; Weinstein, J.A.; Williams, J.A.G. Lighting the way to see inside the live cell with luminescent transition metal complexes. *Coord. Chem. Rev.* **2012**, *256*, 1762–1785. [CrossRef]
10. Fernández-Moreira, V.; Thorp-Greenwood, F.L.; Coogan, M.P. Application of d6 transition metal complexes in fluorescence cell imaging. *Chem. Commun.* **2010**, *46*, 186–202. [CrossRef]
11. Zhang, S.; Hosaka, M.; Yoshihara, T.; Negishi, K.; Iida, Y.; Tobita, S.; Takeuchi, T. Phosphorescent Light-Emitting Iridium Complexes Serve as a Hypoxia-Sensing Probe for Tumor Imaging in Living Animals. *Cancer Res.* **2010**, *70*, 4490–4498. [CrossRef]
12. Venkatesh, V.; Berrocal-Martin, R.; Wedge, C.J.; Romero-Canelón, I.; Sanchez-Cano, C.; Song, J.-I.; Coverdale, J.P.C.; Zhang, P.; Clarkson, G.J.; Habtemariam, A.; et al. Mitochondria-targeted spin-labelled luminescent iridium anticancer complexes. *Chem. Sci.* **2017**, *8*, 8271–8278. [CrossRef] [PubMed]

13. Hwang, H.; Kim, J.; Jeong, J.; Chang, S. Regioselective Introduction of Heteroatoms at the C-8 Position of Quinoline N-Oxides: Remote C–H Activation Using N-Oxide as a Stepping Stone. *J. Am. Chem. Soc.* **2014**, *136*, 10770–10776. [[CrossRef](#)]
14. Hettterscheid, D.G.H.; Kaiser, J.; Reijerse, E.; Peters, T.P.J.; Thewissen, S.; Blok, A.N.J.; Smits, J.M.M.; de Gelder, R.; de Bruin, B. IrII(ethene): Metal or Carbon Radical? *J. Am. Chem. Soc.* **2005**, *127*, 1895–1905. [[CrossRef](#)]
15. Theron, M.; Purcell, W.; Basson, S.S. ([eta]4-Cycloocta-1,5-diene)(2-pyridinethiolato N-oxide-[kappa]O,[kappa]S)iridium(I). *Acta Crystallogr. Sect. C* **1996**, *52*, 336–338. [[CrossRef](#)]
16. Turlington, C.R.; White, P.S.; Brookhart, M.; Templeton, J.L. Oxygen Atom Transfer to a Half-Sandwich Iridium Complex: Clean Oxidation Yielding a Molecular Product. *J. Am. Chem. Soc.* **2014**, *136*, 3981–3994. [[CrossRef](#)] [[PubMed](#)]
17. Hernández, Y.A.; López-Serrano, J.; Paneque, M.; Poveda, M.L.; Vattier, F.; Salazar, V.; Álvarez, E.; Carmona, E. C–N Bond Formation by O₂-Mediated Dehydrogenative Coupling of Phenyl and NH-pyridylidene Ligands on TpIrIII Complexes. *Chem.—A Eur. J.* **2011**, *17*, 9302–9305. [[CrossRef](#)] [[PubMed](#)]
18. Liu, D.; Lu, Y.; Lin, Y.-J.; Jin, G.-X. Donor–Acceptor [2]- and [3]Catenanes Assembled from Versatile Pre-Organized Cp*Rh/Ir-Directed Pseudorotaxane Tectons. *Chem.—A Eur. J.* **2019**, *25*, 14785–14789. [[CrossRef](#)]
19. Shopov, D.Y.; Sharninghausen, L.S.; Sinha, S.B.; Mercado, B.Q.; Brudvig, G.W.; Crabtree, R.H. Modification of a pyridine-alkoxide ligand during the synthesis of coordination compounds. *Inorg. Chim. Acta* **2019**, *484*, 75–78. [[CrossRef](#)]
20. Carlin, R.L.; De Jongh, L.J. Structural and magnetic properties of transition metal complexes of pyridine N-oxide. *Chem. Rev.* **1986**, *86*, 659–680. [[CrossRef](#)]
21. Karayannis, N.M.; Pytlewski, L.L.; Mikulski, C.M. Metal complexes of aromatic amine n-oxides. *Coord. Chem. Rev.* **1973**, *11*, 93–159. [[CrossRef](#)]
22. Henkelis, J.J.; Barnett, S.A.; Harding, L.P.; Hardie, M.J. Coordination Polymers Utilizing N-Oxide Functionalized Host Ligands. *Inorg. Chem.* **2012**, *51*, 10657–10674. [[CrossRef](#)]
23. Puttreddy, R.; Steel, P.J. Synthesis and X-ray crystal structures of silver complexes of 2,6-dimethylpyridine N-oxide: Steric factors override electronic effects. *Polyhedron* **2014**, *69*, 25–30. [[CrossRef](#)]
24. Xu, X.; Zhao, H.; Xu, J.; Chen, C.; Pan, Y.; Luo, Z.; Zhang, Z.; Li, H.; Xu, L. Rhodium(III)-Catalyzed Oxidative Annulation of 2,2'-Bipyridine N-Oxides with Alkynes via Dual C–H Bond Activation. *Org. Lett.* **2018**, *20*, 3843–3847. [[CrossRef](#)]
25. Shahsavari, H.R.; Babadi Aghakhanpour, R.; Hossein-Abadi, M.; Kia, R.; Halvagar, M.R.; Raithby, P.R. Reactivity of a new aryl cycloplatinated(ii) complex containing rollover 2,2'-bipyridine N-oxide toward a series of diphosphine ligands. *New J. Chem.* **2018**, *42*, 9159–9167. [[CrossRef](#)]
26. Puttreddy, R.; Cottam, J.R.A.; Steel, P.J. Anion dependent silver(i) complexes of pyrazine mono-N-oxide. *RSC Adv.* **2014**, *4*, 22449–22454. [[CrossRef](#)]
27. Dadkhah Aseman, M.; Nikravesh, M.; Abbasi, A.; Shahsavari, H.R. Oxidative Addition of a Hypervalent Iodine Compound to Cycloplatinated(II) Complexes for the C–O Bond Construction: Effect of Cyclometalated Ligands. *Inorg. Chem.* **2021**, *60*, 18822–18831. [[CrossRef](#)]
28. Li, Q.-Q.; Kang, Y.-F.; Ren, C.-Y.; Yang, G.-P.; Liu, Q.L.P.; Wang, Y.-Y. Reaction-controlled assemblies and structural diversities of seven Co(ii)/Cu(ii) complexes based on a bipyridine-dicarboxylate N-oxide ligand. *CrystEngComm* **2015**, *17*, 775–786. [[CrossRef](#)]
29. Chen, L.-Z.; Wang, F.-M.; Shu, H. Construction of three metal-organic frameworks based on multifunctional T-shaped tripodal ligands (4,5-dicarboxy-1H-imidazol-2-yl)pyridine-1-oxide. *J. Coord. Chem.* **2012**, *65*, 439–452. [[CrossRef](#)]
30. Ravindran Durai Nayagam, B.; Jebas, S.R.; Edward Rajkumar, J.P.; Schollmeyer, D. Tetraaquabis[3-(2-pyridylsulfanyl)propionato N-oxide]nickel(II). *Acta Crystallogr. Sect. E* **2009**, *65*, m470. [[CrossRef](#)] [[PubMed](#)]
31. Pailloux, S.; Binyamin, I.; Deck, L.M.; Hay, B.P.; Duesler, E.N.; Zakharov, L.N.; Scott Kassel, W.; Rheingold, A.L.; Paine, R.T. Unexpected chelation interaction for 2-hydroxy-2-(1-oxy-pyridin-2-yl)-N,N-diphenyl acetamide with La(III). *Polyhedron* **2009**, *28*, 3979–3984. [[CrossRef](#)]
32. Zucker, S.P.; Wossidlo, F.; Weber, M.; Lentz, D.; Tzschucke, C.C. Palladium-Catalyzed Directed Halogenation of Bipyridine N-Oxides. *J. Org. Chem.* **2017**, *82*, 5616–5635. [[CrossRef](#)] [[PubMed](#)]
33. Xing, J.-N.; Zhang, Y.-P.; Han, S.-J.; Li, B. Synthesis, Crystal Structures, and Characterization of Two New Complexes Constructed From Acipimox Ligands: Two Three-Dimensional Networks Formed Via Hydrogen Bonding. *Synth. React. Inorg. Met.-Org. Nano-Met. Chem.* **2016**, *46*, 409–413. [[CrossRef](#)]
34. Penconi, M.; Cazzaniga, M.; Panzeri, W.; Mele, A.; Cargnoni, F.; Ceresoli, D.; Bossi, A. Unraveling the Degradation Mechanism in Flrpic-Based Blue OLEDs: II. Trap and Detect Molecules at the Interfaces. *Chem. Mater.* **2019**, *31*, 2277–2285. [[CrossRef](#)]
35. You, Y.; Park, S.Y. Inter-Ligand Energy Transfer and Related Emission Change in the Cyclometalated Heteroleptic Iridium Complex: Facile and Efficient Color Tuning over the Whole Visible Range by the Ancillary Ligand Structure. *J. Am. Chem. Soc.* **2005**, *127*, 12438–12439. [[CrossRef](#)] [[PubMed](#)]
36. Bevernaegie, R.; Wehlin, S.A.M.; Piechota, E.J.; Abraham, M.; Philouze, C.; Meyer, G.J.; Elias, B.; Troian-Gautier, L. Improved Visible Light Absorption of Potent Iridium(III) Photo-oxidants for Excited-State Electron Transfer Chemistry. *J. Am. Chem. Soc.* **2020**, *142*, 2732–2737. [[CrossRef](#)] [[PubMed](#)]
37. De Angelis, F.; Fantacci, S.; Evans, N.; Klein, C.; Zakeeruddin, S.M.; Moser, J.-E.; Kalyanasundaram, K.; Bolink, H.J.; Grätzel, M.; Nazeeruddin, M.K. Controlling Phosphorescence Color and Quantum Yields in Cationic Iridium Complexes: A Combined Experimental and Theoretical Study. *Inorg. Chem.* **2007**, *46*, 5989–6001. [[CrossRef](#)]

38. Kim, C.S.; Tinker, L.L.; DiSalle, B.F.; Gomez, E.D.; Lee, S.; Bernhard, S.; Loo, Y.-L. Altering the Thermodynamics of Phase Separation in Inverted Bulk-Heterojunction Organic Solar Cells. *Adv. Mater.* **2009**, *21*, 3110–3115. [[CrossRef](#)]
39. Apex3, Bruker AXS Inc.: Madison, WI, USA, 2015.
40. Sheldrick, G.M. Crystal structure refinement with SHELXL. *Acta Crystallogr. Sect. C Struct. Chem.* **2015**, *71*, 3–8. [[CrossRef](#)]
41. Bernier, D.; Wefelscheid, U.K.; Woodward, S. Properties, Preparation and Synthetic Uses of Amine N-Oxides. An Update. *Org. Prep. Proced. Int.* **2009**, *41*, 173–210. [[CrossRef](#)]
42. Shevlin, M.R.; Stumbo, E.E.; McMillen, C.D.; Pienkos, J.A. Bis[3,5-difluoro-2-(pyridin-2-yl)phenyl](4,4'-dimethoxy-2,2'-bipyridine)iridium(III) hexafluoridophosphate. *IUCrData* **2022**, *7*, x220830. [[CrossRef](#)]
43. Li, X.; Tong, X.; Yin, Y.; Yan, H.; Lu, C.; Huang, W.; Zhao, Q. Using highly emissive and environmentally sensitive o-carborane-functionalized metallophosphors to monitor mitochondrial polarity. *Chem. Sci.* **2017**, *8*, 5930–5940. [[CrossRef](#)]
44. Moriuchi, T.; Katano, C.; Hirao, T. Poly(l-glutamic acid)-modulated Emission Properties of Iridium(III) Complexes in an Aqueous Media. *Chem. Lett.* **2012**, *41*, 310–312. [[CrossRef](#)]
45. Łukomska, M.; Rybarczyk-Pirek, A.J.; Jabłoński, M.; Palusiak, M. The nature of NO-bonding in N-oxide group. *Phys. Chem. Chem. Phys.* **2015**, *17*, 16375–16387. [[CrossRef](#)]
46. Kim, Y.-I.; Song, Y.-K.; Kang, S.K. (5-Methylpyrazine-2-carboxylato-[kappa]2N1,O)bis[2-(4-methylpyridin-2-yl-[kappa]N)-3,5-bis(trifluoromethyl)phenyl-[kappa]C1]iridium(III) chloroform hemisolvate. *Acta Crystallogr. Sect. E* **2014**, *70*, m34. [[CrossRef](#)]
47. Hasan, K.; Bansal, A.K.; Samuel, I.D.W.; Roldán-Carmona, C.; Bolink, H.J.; Zysman-Colman, E. Tuning the Emission of Cationic Iridium (III) Complexes Towards the Red Through Methoxy Substitution of the Cyclometalating Ligand. *Sci. Rep.* **2015**, *5*, 12325. [[CrossRef](#)]
48. Thamilarasan, V.; Karunakaran, P.; Kavitha, N.; Selvaraju, C.; Sengottuvelan, N. Red emitting cyclometallated iridium(III) complexes: Synthesis, characterization and evaluation of biological activities. *Polyhedron* **2016**, *118*, 12–24. [[CrossRef](#)]
49. Song, M.; Yun, S.-J.; Nam, K.-S.; Liu, H.; Gal, Y.-S.; Lee, J.W.; Jin, S.-H.; Lee, J.Y.; Kang, S.K.; Kim, Y.I. Highly efficient solution-processed pure red phosphorescent organic light-emitting diodes using iridium complexes based on 2,3-diphenylquinoxaline ligand. *J. Organomet. Chem.* **2015**, *794*, 197–205. [[CrossRef](#)]
50. Li, G.-N.; Gao, C.-W.; Chen, H.-H.; Chen, T.-T.; Xie, H.; Lin, S.; Sun, W.; Chen, G.-Y.; Niu, Z.-G. Color tuning of cyclometalated 2-phenylbenzo[d]oxazole-based iridium(III) complexes through modification of different N^o ancillary ligands. *Inorg. Chim. Acta* **2016**, *445*, 22–27. [[CrossRef](#)]
51. Thamilarasan, V.; Jayamani, A.; Manisankar, P.; Kim, Y.-I.; Sengottuvelan, N. Green-emitting phosphorescent iridium(III) complex: Structural, photophysical and electrochemical properties. *Inorg. Chim. Acta* **2013**, *408*, 240–245. [[CrossRef](#)]
52. Seo, H.-J.; Heo, Y.-M.; Jin, S.-H.; Soo Yook, K.; Yeob Lee, J.; Kwon Kang, S.; Kim, Y.-I. New heteroleptic cyclometalated iridium(III) complexes containing 2-(2',4'-difluorophenyl)-4-methylpyridine for organic light-emitting diode applications. *J. Lumin.* **2010**, *130*, 1694–1701. [[CrossRef](#)]
53. Bevernaegie, R.; Marcélis, L.; Laramée-Milette, B.; De Winter, J.; Robeyns, K.; Gerbaux, P.; Hanan, G.S.; Elias, B. Trifluoromethyl-Substituted Iridium(III) Complexes: From Photophysics to Photooxidation of a Biological Target. *Inorg. Chem.* **2018**, *57*, 1356–1367. [[CrossRef](#)] [[PubMed](#)]
54. Bünzli, A.M.; Housecroft, C.E.; Constable, E.C.; Zampese, J.A. *CCDC 1853180: Experimental Crystal Structure Determination*; The Cambridge Crystallographic Data Centre: Cambridge, UK, 2018. [[CrossRef](#)]
55. Li, M.-J. *CCDC 2073478: Experimental Crystal Structure Determination*; The Cambridge Crystallographic Data Centre: Cambridge, UK, 2021. [[CrossRef](#)]
56. Baranoff, E.; Bolink, H.J.; Constable, E.C.; Delgado, M.; Häussinger, D.; Housecroft, C.E.; Nazeeruddin, M.K.; Neuburger, M.; Ortí, E.; Schneider, G.E.; et al. Tuning the photophysical properties of cationic iridium(III) complexes containing cyclometallated 1-(2,4-difluorophenyl)-1H-pyrazole through functionalized 2,2'-bipyridine ligands: Blue but not blue enough. *Dalton Trans.* **2013**, *42*, 1073–1087. [[CrossRef](#)] [[PubMed](#)]
57. Baschieri, A.; Sambri, L.; Mazzanti, A.; Carlone, A.; Monti, F.; Armaroli, N. Iridium(III) Complexes with Fluorinated Phenyl-tetrazoles as Cyclometalating Ligands: Enhanced Excited-State Energy and Blue Emission. *Inorg. Chem.* **2020**, *59*, 16238–16250. [[CrossRef](#)]

Disclaimer/Publisher's Note: The statements, opinions and data contained in all publications are solely those of the individual author(s) and contributor(s) and not of MDPI and/or the editor(s). MDPI and/or the editor(s) disclaim responsibility for any injury to people or property resulting from any ideas, methods, instructions or products referred to in the content.